Journal of Neuroinflammation

RESEARCH Open Access

Enhancing TREM2 expression activates microglia and modestly mitigates tau pathology and neurodegeneration

Kai Chen[1†], Fuyao Li[1†], Shuwen Zhang[2], Yixing Chen[1], Tadafumi C. Ikezu[2], Zonghua Li[1], Yuka A. Martens[1], Wenhui Qiao[1], Axel Meneses[1,3], Yiyang Zhu[1], Gisela Xhafkollari[1,4], Guojun Bu[1,5] and Na Zhao[1,3,4*]

Abstract

TREM2, a microglia-specific receptor, is strongly associated with Alzheimer's disease (AD) risk, mediating microglial responses to amyloid pathology critical to AD development. However, its role in tau pathology and neurodegeneration remains unclear. Using the PS19 tauopathy mouse model with inducible overexpression of human wild-type TREM2 (TREM2-WT) or the R47H variant (TREM2-R47H), we show that increasing TREM2-WT expression modestly reduces soluble phosphorylated tau levels and mildly preserves neuronal integrity. Single-cell RNA sequencing reveals that TREM2-WT robustly enhances microglial activation, characterized by a disease-associated microglia (DAM) signature. In contrast, TREM2-R47H overexpression exhibits a loss-of-function phenotype, with no significant impact on tau levels, neurodegeneration, or microglial activation. These findings highlight the role of TREM2 in modulating microglial activity and its influence on tau pathology and neurodegeneration, providing important insights for the future development of therapies targeting TREM2 or microglial pathways in AD or other tauopathies.

Keywords TREM2, R47H variant, Microglia, Alzheimer's disease, Tau pathology, Transcriptomics

Introduction

Alzheimer's disease (AD) is a chronic neurodegenerative disorder characterized by the deposition of extracellular amyloid-β (Aβ) plaques and the accumulation of neurofibrillary tangles composed of aggregated tau proteins within neurons [1, 2]. A hallmark of AD pathology is the activation of microglia, particularly around amyloid plaques [3]. Genetic studies have identified several immune-related genes as risk factors for late-onset AD, with the triggering receptor expressed on myeloid cells 2 (*TREM2*) among the most significant. TREM2 variants such as TREM2-R47H substantially increase the risk of developing late-onset AD [4, 5].

TREM2 is a cell surface receptor in the immunoglobulin superfamily, predominantly expressed in myeloid cells such as microglia in the brain [6]. When bound to its

†Kai Chen and Fuyao Li contributed equally to this work.

*Correspondence:
Na Zhao
zhao.na@mayo.edu
[1]Department of Neuroscience, Mayo Clinic, 4500 San Pablo Road, Jacksonville, FL 32224, USA
[2]Department of Quantitative Health Sciences, Mayo Clinic, Jacksonville, FL, USA
[3]Clinical and Translational Science Graduate Program, Mayo Clinic, Jacksonville, FL, USA
[4]Neuroscience Graduate Program, Mayo Clinic, Jacksonville, FL, USA
[5]Division of Life Science and State Key Laboratory of Molecular Neuroscience, The Hong Kong University of Science and Technology, Clear Water Bay, Hong Kong, China

ligands such as lipids, apolipoprotein E (APOE), and Aβ, TREM2 initiates signaling through its adaptor proteins, DAP12 or DAP10, activating downstream pathways that regulate microglial survival and activation [7–13]. Multiple studies have shown that TREM2 is a key driver of disease-associated microglia (DAM) phenotypes, playing a critical role in microglial responses to Aβ, including its seeding and clearance [14–17]. TREM2 deficiency restricts microglia in a homeostatic state and dampens their response to pathological cues like Aβ [15, 16, 18]. On the other hand, elevating TREM2 levels [17, 19] or signaling [20, 21] ameliorates amyloid pathogenesis, particularly in the early stage of amyloid development, with TREM2-R47H exhibiting a loss-of-function effect. Additionally, TREM2 agonist antibody activates microglia and reduces amyloid burden in amyloid mouse models [22–24], suggesting a promising therapeutic potential for AD treatment.

While the role of TREM2 in Aβ pathology is well-documented, its influence on tau pathology remains controversial. Some studies suggest that TREM2 knockout (KO) or the TREM2-R47H variant has a protective effect by reducing tau pathology through dampened microglial responses [25, 26]. On the other hand, sustained microglial activation via TREM2 agonist antibody treatment has been shown to exacerbate Aβ-induced tau pathology [27]. Conversely, other studies indicate that TREM2 deletion exacerbates tau accumulation and spreading, while promoting brain atrophy, suggesting a protective role for TREM2 signaling in tau pathogenesis [28–30]. Notably, two other studies found that complete deletion of the murine *Trem2* gene does not significantly affect tau pathology in PS19 mice [26, 31]. These conflicting results point to the need for further research to clarify whether targeting TREM2 could have therapeutic potential in influencing tau pathology and related neurodegeneration.

To address this, we employed microglia-specific inducible mouse models with controlled expression of either human wild-type TREM2 (TREM2-WT) or the R47H variant (TREM2-R47H). Previously, using these inducible mice on a 5xFAD background, we demonstrated that elevating TREM2 expression mitigates early amyloid development [17]. In this study, we crossed these TREM2-inducible mice with PS19 tauopathy models. Our findings show that increased TREM2-WT expression mildly reduced phosphorylated tau levels and neurodegeneration, accompanied by significant DAM activation revealed by single cell RNA sequencing (scRNA-seq). In contrast, elevated TREM2-R47H expression exhibited a loss-of-function phenotype, showing no significant effects on tau pathology or DAM activation. Collectively, our study suggests that enhancing TREM2 expression activates microglia and provides modest protective effects on tau pathology and neuronal integrity.

Methods

Mouse models

The cell-type-specific inducible human TREM2-WT or TREM2-R47H mouse models were generated by a knock-in strategy targeting the *Rosa26* locus as previously described [17]. To establish microglial-specific TREM2 expressing animal models in tau background, the inducible TREM2-WT and TREM2-R47H mice were bred with Cx3cr1^{CreER} mice (stock# 021160; The Jackson Laboratory), and further crossed with PS19 (with *MAPT*-P301S mutation) model mice (stock# 008169; The Jackson Laboratory) and established *MAPT-P301S*$^{+/-}$; *TREM2-WT*$^{+/+}$; *Cx3cr1*$^{CreER/+}$ mice (referred to as PS19-TREM2-WT) and *MAPT-P301S*$^{+/-}$; *TREM2-R47H*$^{+/+}$; *Cx3cr1*$^{CreER/+}$ mice (referred to as PS19-TREM2-R47H).

To induce the expression of TREM2-WT or TREM2-R47H, the mice at 1.5 months of age were administered two doses of 250 mg/kg tamoxifen via gavage, with a separation of 48-hour between doses (referred to as induced) [32]. The control groups received an equivalent volume of corn oil (referred to as Ctrl). Both male and female mice were used in the experiments. The animal housing conditions were in accordance with the Guide for the Care and Use of Laboratory Animals (temperature of 68–79 °F; 30–70% relative humidity).

Tissue Preparation

Mice were deeply anesthetized with isoflurane prior to transcardial perfusion with Phosphate Buffered saline (PBS, Cat# BP39920, Fisher BioReagents). The brains were extracted and divided along the midline. For immunostaining analyses, one-half of the brain was fixed in 4% paraformaldehyde (PFA, Cat# sc-281692, Santa Cruz) at 4 °C overnight and then transferred to 30% sucrose (Cat# S7903, Sigma-Aldrich) solution for 48 h. The tissues were subsequently embedded in O.C.T. compound (Cat# 23-730-571, Fisher Healthcare) and snap-frozen in liquid nitrogen prior to cryostat sectioning. The other half of the brain was dissected to isolate the cortical and hippocampal regions, which were snap-frozen in liquid nitrogen and kept at -80 °C until used for extraction and biochemical analyses. A three-step sequential extraction process was conducted. First, brain tissues were homogenized and lysed in RAB buffer (Cat# 786 – 91, G-Biosciences), supplemented with protease inhibitor (Cat# 11697498001, cOmplete, Roche) and phosphatase inhibitor (Cat# 4906845001, PhosSTOP, Roche). The homogenates were centrifuged at 50,000 × g for 20 min at 4 °C, and the resulting supernatants were collected as RAB-soluble fractions. The pellets were re-suspended in RIPA buffer (Cat# 20–188, Millipore) with added protease inhibitor (Cat# 11697498001, cOmplete, Roche) and phosphatase inhibitor (Cat# 4906845001, PhosSTOP, Roche), followed by centrifugation at 50,000 × g

for 20 min at 4 °C. The supernatants from this step were collected as RIPA-soluble fractions. Finally, the remaining pellets were suspended in 70% formic acid (FA) and centrifuged again at 50,000 × g for 20 min at 4 °C. The supernatants were collected as FA fractions. All extracted fractions were stored at -80 °C until used for western blot and ELISA analyses.

Western blotting

Equal amounts of protein from the RAB and RIPA fractions were resolved by SDS-polyacrylamide gel electrophoresis (SDS-PAGE) and transferred onto polyvinylidene difluoride membranes (PVDF, Cat# IPFL00010, Millipore). After blocking with 5% nonfat milk, the membrane was incubated with primary antibodies at 4 °C overnight and horseradish peroxidase (HRP)-conjugated secondary antibodies at room temperature for 1 h. Chemiluminescence was detected using ECL Substrate (Pierce). Immunoblots were visualized using the Bio-Rad ChemiDoc MP imaging system. The following primary antibodies were used: anti-human TREM2 (Cat# 91068, Cell Signaling Technology, 1:1,000), and anti-β-actin (Cat# A2228, Sigma-Aldrich, 1:2,000) antibodies.

ELISA

The levels of total tau in RAB, RIPA and FA fractions were quantified by sandwich ELISA as previously described [33], using a monoclonal tau antibody (HT7, Cat# MN1000, Thermo Scientific) as the capture antibody and a biotin-conjugated tau antibody (BT2, Cat# MN1010B, Thermo Scientific) as the detection antibody. Phospho-tau (pT181) was determined by Phospho-Tau ELISA Kit (Cat# KHO0631, Thermo Scientific) according to the manufacturer's instruction. Briefly, standards and samples were diluted with Standard Diluent Buffer and added into the antibody-coated plate. Then, add 50 µL Detection Antibody solution into each well and incubated overnight at 4 °C. After washing, the plate was incubated with 100 µL 1X Anti-Rabbit IgG HRP solution for 30 min. After washing, add 100 µL Stabilized Chromogen to each well. After incubating for 30 min at room temperature in the dark, add 100 µL Stop Solution to each well and read the absorbance at 450 nm.

Immunofluorescence staining

Brain sections (40 µm thickness; coronal) were collected from the same brain region for all the animals, and brain regions were confirmed under the microscope by comparing sections to images on the Allen Mouse Brain Atlas (http://mouse.brain-map.org). The sections were placed into a 48-well plate for free-floating immunostaining. After blocked in 5% goat serum (Cat# S-1000, Vector Laboratories) for 1 h, sections were incubated with the primary antibodies overnight. Sections were then incubated with Alexa Fluor-conjugated secondary antibodies for 2 h at room temperature (1:1,000; Invitrogen). The following primary antibodies were used: anti-phospho-tau at site Ser202 and Thr205 (Cat# MN1020, AT8, Thermo Fisher Scientific, 1:500); anti-human TREM2 (16E1, produced in-house at Mayo Clinic, 1:500) [17]; anti-IBA1 (Cat# 019-19741, Wako, 1:1,000); anti-NeuN (Cat# MAB377, clone A60, Millipore, 1:1,000); anti-Galectin 3 (Cat# 14-5301-82, Thermo Fisher Scientific,1:300), MC-1 (1:100, gift from Dr. Peter Davies [34]).

Image acquisition and quantification

Immunofluorescence images were acquired using a Carl Zeiss (LSM800) confocal microscope at 20X magnification with consistent laser and detector settings. 30-µm Z-stacks (20 optical slices, 1.5-µm thickness each) were collected, and maximum intensity projections were generated. Other fluorescent images were captured using Keyence (BZ-X810) or Phenoimager HT microscopes at 20X magnification, with autofocus performed under identical settings within each experiment. For each staining, the hippocampus and piriform cortex were manually traced and saved as Regions of Interest (ROIs) using ImageJ. A unified intensity threshold was applied across all samples within each staining. Pixels exceeding this threshold were quantified to determine the percentage of positive immunoreactive area using the particle analysis plugin. The thickness of the layered hippocampal structures CA1 and DG was determined by measuring the average width of each structure using ImageJ.

RNA isolation and real-time PCR analysis

Total RNA was isolated by using Trizol (Cat# 15596018, Thermo Fisher Scientific), RNeasy Mini Kit (Cat# 74104, QIAGEN) and subjected to DNase I (Cat# 79254, QIAGEN) digestion to remove contaminating genomic DNA. Reverse transcription was performed using iScript™ Reverse Transcription Supermix (Cat# 1708891, Bio-Rad). cDNA was added to a reaction mix (10 µL final volume) containing gene-specific primers and SYBR green supermix (Cat# 172–5274, Bio-Rad). All samples were run in duplicates and were analyzed with QuantStudio 7 Flex Real-Time PCR System (Thermo Fisher Scientific). The relative gene expression was normalized to actin controls and assessed using the $2^{-\Delta\Delta CT}$ method. Primer sequences and information are as follows (5′-3′): murine actin: 5′- AGTGTGACGTTGACATCCGTA-3′ (forward) and 5′-GCCAGAGCAGTAATCTCCTTC-3′ (reverse); human TREM2: 5′-GCTGCTCATCTTACTCTTTGTC-3′ (forward) and 5′-TCATAGGGGCAAGACACCT-3′ (reverse); murine Trem2: 5′-GCACCTCCAGGAATCAAGAG-3′ (forward) and 5′-GGGTCCAGTGAGGATCTGAA-3′ (reverse); total TREM2/Trem2: 5′-GCCCAT

GCCAGCGTGTGGT-3′ (forward) and 5′-CACTGG TAGAGGCCCGC-3′ (reverse).

Single cell isolation and sequencing

The single cell isolation and scRNA-seq analyses were performed as we described [17]. Briefly, isoflurane was used to anesthetize mice before transcardial perfusion with PBS. The cortical tissues were quickly dissected and enzymatically digested using the Neural Tissue Dissociation kit (P) (Cat# 130-092-628, Miltenyi Biotec). Myelin was removed using magnetic bead separation (Myelin Removal Beads II, Cat# 130-096-733, Miltenyi Biotec) followed by the red blood cell lysis (Cat# 130-094-183; Miltenyi Biotec) and dead cell removal (Cat# 130-090-101; Miltenyi Biotec) according to the manufacturer's instructions. The final cell pellet was suspended in Ca/Mg-free PBS supplemented with 0.5% FBS. Trypan blue examination confirmed that over 90% of the cells were viable in each sample.

ScRNA-seq was conducted using the Chromium platform (10x Genomics) with the 3′ Gene Expression V3 kit, targeting an input of approximately 7,000 cells per sample. In summary, gel beads in emulsions (GEMs) were generated on the sample chip using the Chromium Controller. Barcoded cDNA was extracted from the GEMs through Post-GEM RT-cleanup and subsequently amplified for 12 cycles. The amplified cDNA underwent fragmentation, end-repair, poly-A tailing, adaptor ligation, and 10x-specific sample indexing according to the manufacturer's protocol. Library quality was assessed using the TapeStation (Agilent), and libraries were sequenced on a HiSeq 4000 instrument (Illumina), aiming for a sequencing depth of 25,000 to 50,000 reads per cell.

ScRNA-seq data analysis

scRNA-seq data were processed using the standard 10x Genomics Cell Ranger Single Cell Software Suite (v3.0.0). In brief, raw sequencing reads were demultiplexed, aligned to the mm10 reference mouse genome, and the reads aligned to each gene were counted. Cell filtration, normalization, clustering and differential expression analyses were performed using standard Seurat package procedures (v.4.0) with default parameter settings. For quality control, cells that had unique gene counts over 6,000 or less than 200 and >20% mitochondrial content were removed. SCTransform was used to normalize and scale data and to remove the confounding sources of variation of sequencing depth, mitochondria gene percentage, and ribosomal protein gene percentage. All samples were integrated, and canonical correlation analysis was performed to identify common sources of variation among samples and to remove batch effects. The first 30 canonical correlation vectors were used for subsequent clustering analysis and visualization using UMAP. Function "FindAllMarkers" was used to identify cluster-specific genes. Cell clusters were manually annotated as specific cell types based on literature and the datasets for murine cell taxonomy. Cell doublets that expressed more than one cell type marker were excluded from downstream analyses.

The microglia cell clusters were further classified into HM, DAM, IRM, REM, MHCII^{+}, and CPM based on the expression patterns of marker genes [15, 16, 35]. Differentially expressed genes (DEGs) in each pairwise comparison within microglia clusters (PS19-TREM2-WT-induced versus Ctrl or PS19-TREM2-R47H-induced versus Ctrl) were calculated using the MAST test while correcting for sex effects. Genes with adjusted $P<0.05$ and average log 2 fold change >= 1 were defined as significant DEGs. Gene Ontology (GO) enrichment analysis of DEGs from each cluster was performed using R package clusterProfiler [36, 37].

Statistical analyses

All data were reported as mean values ± SEM unless otherwise indicated. Generally, to ensure that results were valid in the presence of non-normal distributions, or differing variances between groups, nonparametric Mann-Whitney test was used to compare outcomes among groups when sample size is larger than 10. With the sample size ≤ 10, since nonparametric tests would have very low power, a Student's *t* test was used to compare outcomes among groups. Statistics were analyzed using GraphPad Prism v10.0.0. All statistical tests were two-sided. The statistical tests used for each analysis, the sample size, and the significance levels were reported in the caption of each figure.

Results

Characterization of microglia-specific PS19-TREM2 inducible mouse models

To investigate the effects of human TREM2 on microglial function, we previously generated inducible mouse models that conditionally express human TREM2-WT or TREM2-R47H in a cell-type-specific manner using a Cre-loxP knock-in strategy targeting the *Rosa26* locus [17]. An enhanced green fluorescent protein (EGFP) cDNA was included and expressed under the control of an internal ribosomal entry site, serving as a surrogate marker for human TREM2 expression. These mouse models were then crossed with *Cx3cr1*$^{CreER/+}$ mice to enable microglia-specific expression of human TREM2-WT or TREM2-R47H, along with EGFP, upon tamoxifen (TAM) treatment (Fig. 1A). To further examine the impact of human TREM2-WT and TREM2-R47H on tau pathology and associated neurodegeneration, we crossed the microglia-specific TREM2-WT and TREM2-R47H mice with the PS19 tauopathy model carrying the human

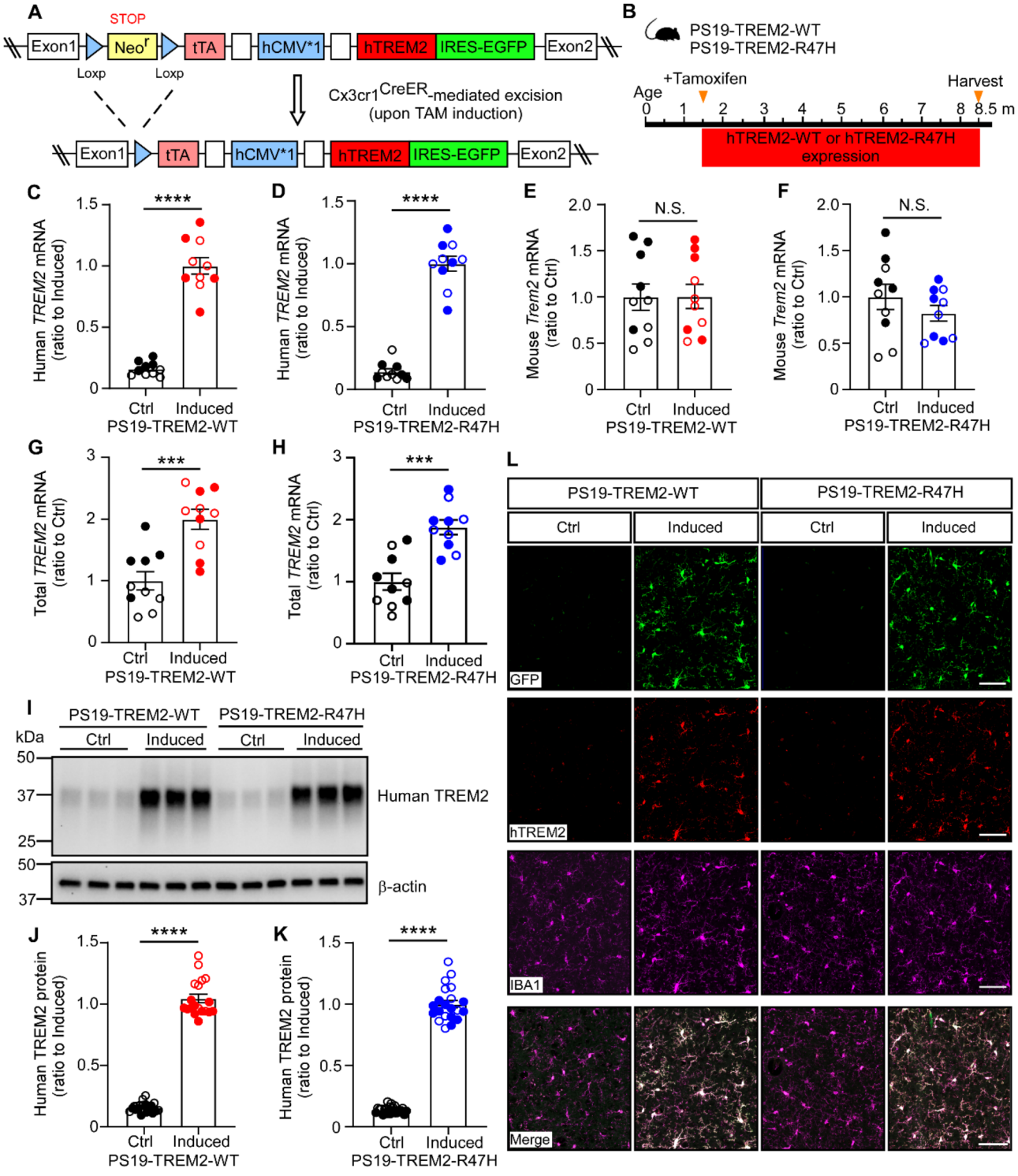

Fig. 1 (See legend on next page.)

(See figure on previous page.)

Fig. 1 Characterization of microglia-specific PS19-TREM2 inducible mouse models

(**A**) Schematic illustrative of the *inducible* expression of TREM2-WT or TREM2-R47H knock-in alleles. The TREM2 floxed mice were bred with the Cx3cr1^{CreER} mice to generate TREM2-WT (*TREM2-WT*$^{+/+}$; *Cx3cr1*$^{CreER/+}$) or TREM2-R47H (*TREM2-R47H*$^{+/+}$; *Cx3cr1*$^{CreER/+}$) mice. Administration of tamoxifen to these mice led to the removal of the loxP-flanked Neo^{r} gene and expression of human TREM2-WT or TREM2-R47H in microglia. (**B**) Illustration of induction paradigms for the expression of human TREM2-WT or TREM2-R47H in the PS19 background. (**C**-**H**) The mRNA levels of human *TREM2* (**C** and **D**), mouse *Trem2* (**E** and **F**), and total *TREM2* (human + mouse; **G** and **H**) in the brain were quantified by qPCR. $n = 10$ mice/group (mixed sexes). In **C**–**H**, each datapoint (circle) represents an individual animal, male and female mice are labeled as solid and open circles, respectively. Two-tailed unpaired Student's *t* tests with Bonferroni correction were used for statistical analysis. *P* values < 0.05 were considered to be statistically significant. ***, $P < 0.001$; ****, $P < 0.0001$; N.S., not significant. Data are mean ± SEM. (**I**-**K**) The protein levels of human TREM2 in the cortical RIPA lysate were quantified by western blot. $n = 19$–23 mice/group (mixed sexes). In **J**-**K**, each datapoint (circle) represents an individual animal, male and female mice are labeled as solid and open circles, respectively. Mann – Whitney tests followed by Bonferroni correction for multiple comparisons were used for statistical analysis. *P* values < 0.05 were considered to be statistically significant. ****, $P < 0.0001$; N.S., not significant. Data are mean ± SEM. (**L**) Representative images of the GFP, human TREM2, and IBA1 co-staining. Scale bar, 50 µm.

MAPT-P301S mutation. This generated *MAPT-P301S*$^{+/-}$; *TREM2-WT*$^{+/+}$; *Cx3cr1*$^{CreER/+}$ (referred to as PS19-TREM2-WT) and *MAPT-P301S*$^{+/-}$; *TREM2-R47H*$^{+/+}$; *Cx3cr1*$^{CreER/+}$ (referred to as PS19-TREM2-R47H) mice (Fig. 1B). In PS19 mice, pathological tau seeding is detected as early as 1.5 months [38], and synapse loss occurs by 3 months of age [39]. To ensure TREM2 expression is induced early enough to coincide with tau seeding and before neurodegeneration begins, while also avoiding potential effects on early brain development, we selected 1.5 months of age as the induction time point. These mice were subjected to either vehicle (referred to as "Ctrl" group) or TAM (referred to as "Induced" group) administration at 1.5 months of age and harvested at 8.5 months of age (Fig. 1B).

Using these new mouse models, we first confirmed significantly higher mRNA levels of human *TREM2-WT* or *TREM2-R47H* in the induced groups compared to their respective Ctrl groups (Fig. 1C, D). The levels of endogenous murine *Trem2* mRNA remained comparable between the Ctrl and induced groups for both TREM2-WT and TREM2-R47H mice (Fig. 1E, F). Using primers designed to detect both human *TREM2* and murine *Trem2* with equal efficiency, thereby reflecting total *TREM2* levels, we found that the induced groups exhibited approximately double the total *TREM2* mRNA levels compared to the Ctrl groups in both TREM2-WT and TREM2-R47H mice (Fig. 1G, H), consistent with our earlier findings [17]. Western blotting analysis further confirmed significantly elevated human TREM2 protein levels in cortical brain RIPA lysates from the induced mice (Fig. 1I–K). As reported by previous studies using the *Cx3cr1*^{CreER} mice [40], we observed approximately 10% spontaneous recombination in the absence of tamoxifen (TAM), evidenced by the qPCR (Fig. 1C, D) and the Western blot signal (Fig. 1I-K) in the control groups. Finally, immunofluorescence co-staining demonstrated that TREM2 and GFP colocalized exclusively with microglia marker Iba1, confirming microglia-specific expression of human TREM2 in our mouse models as designed (Fig. 1L).

TREM2-WT expression in microglia modestly reduces the levels of soluble phosphorylated Tau in PS19 mice

To evaluate tau pathology, we performed immunofluorescence staining for phosphorylated tau (p-tau) using the AT8 antibody on PS19-TREM2 mice at 8.5 months of age. Profound p-tau + pathology was observed in the piriform cortex and hippocampus, consistent with previous reports using the PS19 mouse model [26, 39, 41]. We did not detect significant differences in tau pathology between the PS19-TREM2-WT induced and control groups or between the PS19-TREM2-R47H induced and control groups, in either the piriform cortex (Fig. 2A-C) or the hippocampus (Fig. 2D-F). We also performed immunostaining using the MC-1 antibody, which targets a pathological conformation of tau [34]. Our results with MC-1 are similar to AT8 stanning, showing no significant differences in tau pathology between control and induced groups for both PS19-TREM2-WT and PS19-TREM2-R47H mice (Supplementary Fig. 1A-F). Furthermore, a correlation analysis confirmed a strong positive correlation between AT8 and MC-1 staining results, reinforcing the reliability of our observations (Supplementary Fig. 1G and H). Additionally, we measured the levels of soluble and insoluble p-tau and total tau using ELISA in three brain lysate fractions, including the RAB buffer soluble fraction, RIPA detergent soluble fraction, and formic acid (FA) detergent insoluble fraction (Fig. 2G-R). We found no significant differences in RAB and FA fractions for both p-tau and total tau levels between induced and control animals in either the PS19-TREM2-WT or PS19-TREM2-R47H groups, with the exception that the p-tau level in the RIPA fraction was significantly lower in PS19-TREM2-WT induced mice compared to control mice (Fig. 2K); however, this difference was not observed in PS19-TREM2-R47H mice (Fig. 2L). Both AT8 staining and Elisa results are consistent across female and male mice in a sex-specific analyses (Supplementary Fig. 2 and Supplementary Fig. 3). These results suggest that elevating TREM2-WT expression has a modest impact on tau pathology in our model system.

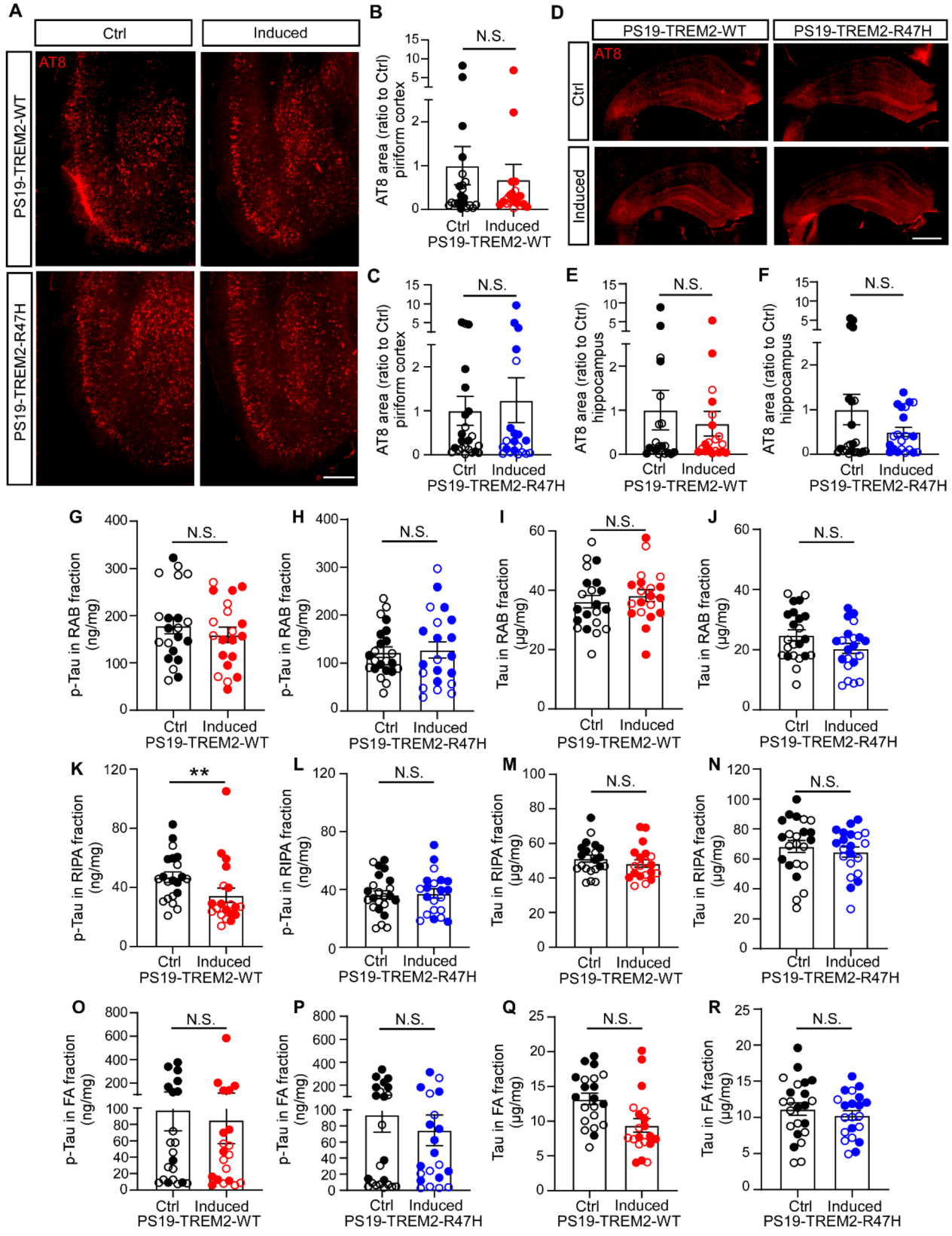

Fig. 2 (See legend on next page.)

(See figure on previous page.)

Fig. 2 The impact of TREM2 expression on tau pathology

(**A**-**C**) Representative images of piriform cortical region (**A**) and quantification (**B** and **C**) of p-tau by immunofluorescence staining with AT8 antibody. Scale bar, 500 µm. (**D**-**F**) Representative images of hippocampus (**D**) and quantification (**E** and **F**) of p-Tau by AT8 immunofluorescence staining. Scale bar, 500 µm. (**G**-**R**) The levels of p-tau and total tau in the buffer soluble (RAB), detergent soluble (RIPA), and insoluble (FA) fractions were detected by ELISAs in the mice with or without TREM2-WT or TREM2-R47H overexpression. Sample size: $n = 19–23$ mice/group, with mixed sexes. Each datapoint (circle) represents an individual animal, male and female mice are labeled as solid and open circles, respectively. Data are shown as mean ± SEM. Mann–Whitney tests were used for statistical analysis. *P* values < 0.05 were considered to be statistically significant. $^{**}P < 0.01$; N.S., not significant.

TREM2-WT expression in microglia leads to mild protection against neurodegeneration in PS19 mice

To further assess the impact of TREM2-WT and TREM2-R47H expression on neurodegeneration in PS19 mice, we conducted immunofluorescence staining for the neuronal marker NeuN and quantified the lateral ventricle area. No differences were observed in the lateral ventricle area between the induced and control groups in either PS19-TREM2-WT or PS19-TREM2-R47H mice (Fig. 3A-C). We then quantified the thickness of the pyramidal neuronal layer in the piriform cortex (Fig. 3D-F), along with neuronal layers thickness in CA1 and the dentate gyrus (DG) within the hippocampus (Fig. 3G-K). In the piriform cortex, the thickness of the pyramidal neuronal layer did not differ significantly between induced and control groups for either PS19-TREM2-WT or PS19-TREM2-R47H mice (Fig. 3D-F). Similarly, the thickness of the neuronal layer in the CA1 region showed no significant differences between the groups (Fig. 3G-I). However, a slight increase in DG layer thickness was observed in the PS19-TREM2-WT induced group compared to its control group (Fig. 3J), a difference not observed in PS19-TREM2-R47H mice (Fig. 3K).

Collectively, our data suggest that the overexpression of TREM2-WT in microglia may have a mild effect on reducing pathological tau levels (Fig. 2) and protecting against neural loss in the hippocampal DG region (Fig. 3) in our model system, whereas TREM2-R47H appears to represent a loss-of-function in these events.

Elevating TREM2-WT expression does not alter microglia density but activates the DAM microglia signature

To investigate the impact of TREM2 expression on microglia in these tau models, we assessed microglia density in the piriform cortex and hippocampus using Iba1 staining. No significant differences in microglial coverage were observed between the PS19-TREM2-WT induced and control groups, or between the PS19-TREM2-R47H induced and control groups, in either the piriform cortex (Fig. 4A-C) or the hippocampus (Fig. 4D-F).

To further explore the microglial molecular signature, we isolated cortical single cells from an independent cohort of animals and performed scRNA-seq analysis, focusing on microglia population for downstream analysis (Fig. 5). After removing other cell types, we recovered a total of 105,136 microglia, which were grouped into 14 distinct clusters following unsupervised clustering. These clusters were visualized using Uniform Manifold Approximation and Projection (UMAP) (Fig. 5A). Based on published microglial subtype-specific marker gene expression data [15–17, 20, 42], we further identified subclusters of microglia, including the homeostatic microglia (HM1-8; high expression of *Cx3cr1*, *P2ry12*, *Tmem119*, *and Csf1r*); disease-associated microglia (DAM1 and DAM2, high expression of high expression of *Tyrobp*, *Apoe*, *Ctsb*, *Fth1*, *Ccl3*, *Ctsl*, *Lpl*, *Cst7*, and *Cd9*); interferon response microglia (IRM, high expression of *Ifit3*, *Isg15*, *Ifitm3*, *and Irf7*), major histocompatibility complex class II expressing microglia (MHCII+, high expression of *H2-Ab1*, *H2-Eb1*, *H2-Aa* and *Cd74*), ribosomal gene enriched microglia (REM, high expression of *Rpl41*, *Rps12*, *Rpl23* and *Rps20*), and cycling/proliferating microglia (CPM; high expression of *Stmn1*,*Top2a*, *Mki67 and Hmgb2*) (Fig. 5B) [15, 20, 43]. The composition of these subclusters was similarly represented in the induced PS19-TREM2-WT and PS19-TREM2-R47H mice compared to their littermate controls (Fig. 5C).

We next focused on differentially expressed genes (DEGs) specifically comparing PS19-TREM2-WT and PS19-TREM2-R47H-induced mice versus their littermate controls (Supplementary Tables 1, 2, 3 and 4). Interestingly, TREM2-WT-induced microglia showed a significant number of DEGs in the DAM subclusters particularly DAM1 cluster (Fig. 5D; Supplementary Table 1). In contrast, transcriptional profiles of TREM2-R47H-induced microglia revealed only a limited number of DEGs, reflecting a reduced response (Fig. 5E; Supplementary Table 2). Pathway analysis of DAM1-specific DEGs in TREM2-WT-induced microglia highlighted terms such as "leukocyte migration", "cell chemotaxis", "positive regulation of response to external stimulus", and "regulation of vasculature development" (Fig. 5F; Supplementary Table 3), emphasizing potential activation driven by TREM2-WT overexpression. In contrast, pathway analysis of DAM1-specific DEGs in TREM2-R47H-induced microglia revealed an opposing regulatory profile, including terms such as "negative regulation of angiogenesis", "negative regulation of vasculature development", and "negative regulation of response to external stimuli" (Fig. 5G; Supplementary Table 4). Comparative gene expression analysis in DAM1 further revealed the strong upregulation of microglial activation genes such as *Lgals3*, *Itga4*, *Spp1*, and *Flt1 and* downregulation of microglial homeostatic genes including *P2ry12*

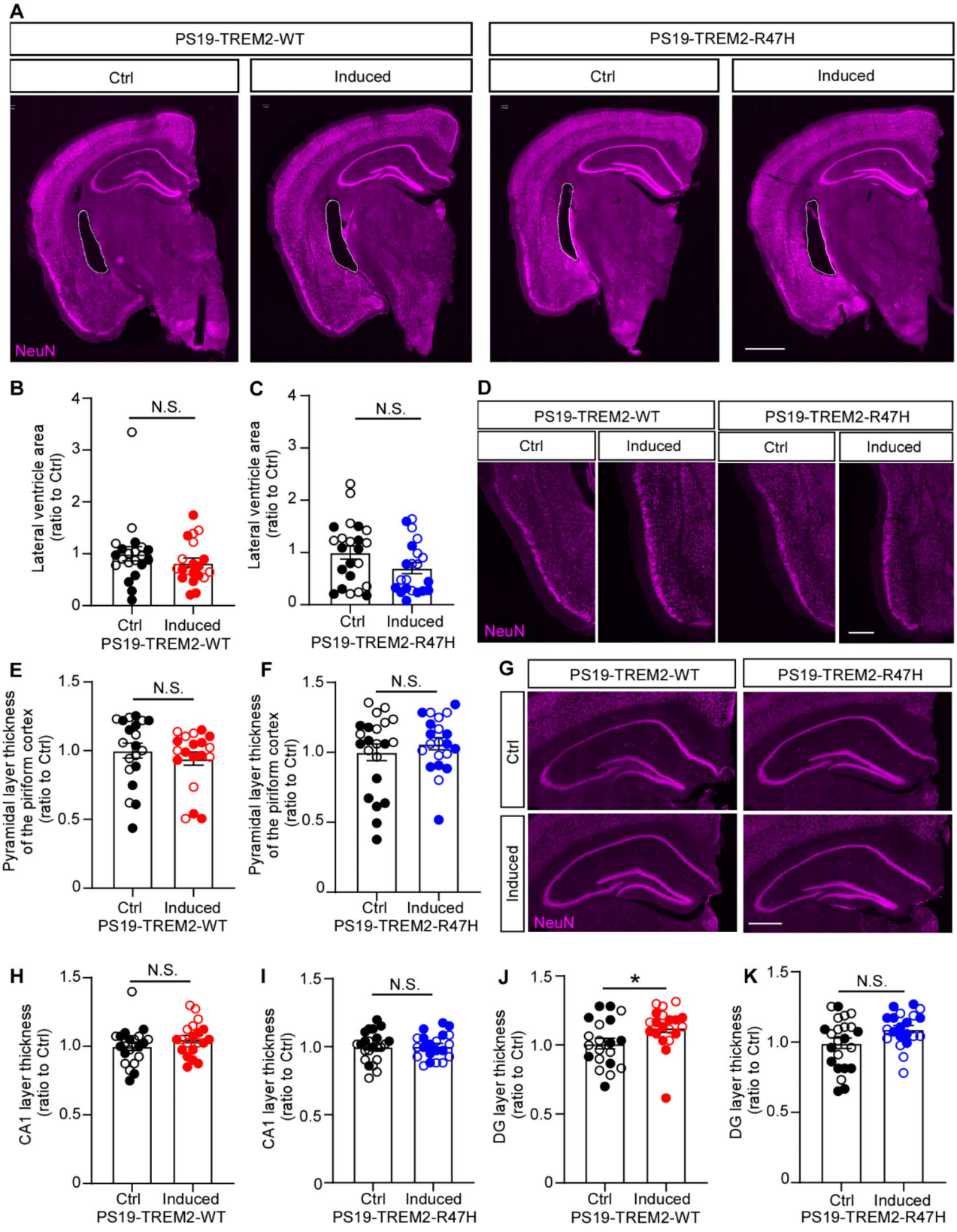

Fig. 3 (See legend on next page.)

(See figure on previous page.)

Fig. 3 The impact of TREM2 expression on neurodegeneration

NeuN immunofluorescence staining was carried out on PS19 mice expressing either TREM2-WT or TREM2-R47H. (**A**-**B**) Representative images (**A**) and quantification (**B** and **C**) of the lateral ventricle area in mice following the induction of TREM2-WT or TREM2-R47H expression in microglia within the PS19 background. Scale bar, 1 mm. (**D**-**F**) Representative images (**D**) and quantification (**E** and **F**) of the thickness of the pyramidal neuronal layer in the piriform cortex in mice upon induction of TREM2-WT or TREM2-R47H expression in microglia within the PS19 background. Scale bar, 500 µm. (**G**-**K**) Representative images (**G**) and quantification (**H**-**K**) of the thickness of the neuronal layers in the in mice following induction of TREM2-WT or TREM2-R47H expression in microglia within the PS19 background. Scale bar, 500 µm. Sample size: $n = 19–23$ mice per group, with mixed sexes. Each datapoint (circle) represents an individual animal, male and female mice are labeled as solid and open circles, respectively. Data are presented as mean ± SEM. Statistical analysis was conducted using Mann–Whitney tests. *P* values less than 0.05 were considered statistically significant. $^*P < 0.05$; N.S., not significant.

in TREM2-WT-induced microglia, with limited changes in TREM2-R47H-induced microglia (Fig. 5H). To further validate these scRNA-seq results, particularly the changes in the DAM microglia signature, we performed Galectin-3 (encoded by *Lgals3* gene) immunostaining using a separate cohort of mice, independent of the scRNA-seq analysis. Consistently, we observed a significant increase of Galectin-3 + microglia in the cortex of TREM2-WT-induced, but not TREM2-R47H-induced mice (Fig. 5I-K).

Overall, our data indicate that elevating TREM2-WT expression strongly enhances DAM-associated phenotypes and activates microglia, while TREM2-R47H shows a reduced capacity to do so. However, these microglial changes driven by TREM2-WT lead to only a modest impact on tau pathology and related neurodegeneration in our models.

Discussion

In this study, we employed a microglia-specific human TREM2 overexpression mouse model to investigate the effects of TREM2-WT and TREM2-R47H on tau pathology, neurodegeneration, and microglial responses. Our findings demonstrate that elevating TREM2-WT expression robustly activates microglia and provides modest benefits for tau pathology, including reductions in soluble p-tau levels and mild preservation of neuronal integrity, but does not affect insoluble p-tau or total tau levels. The reason why only soluble p-tau levels were altered while insoluble tau remained unchanged is unclear. However, since soluble p-tau is considered a potentially toxic early marker of tau pathology and neurodegeneration [44], this suggests that TREM2-mediated microglial activation may have a mild protective effect in the early stages of tau pathogenesis. In contrast, TREM2-R47H expression exhibits a loss-of-function phenotype, with no significant impact on tau pathology, neurodegeneration, or microglial activation.

In tauopathy mouse models such as PS19 mice, microglial activation is one of the earliest changes observed at three months of age, even preceding the onset of tau pathology [39]. However, there is an ongoing debate about whether microglial activation exacerbates or mitigates tau pathology and related neurodegeneration in these models. Studies using different tauopathy mouse models have reported mixed findings when targeting TREM2. Using PS19 mice, some studies suggest that complete deletion of the murine *Trem2* gene does not significantly affect tau pathology [26, 31], whereas others indicate that *Trem2* haploinsufficiency or knockdown exacerbates tau pathology [30, 45, 46]. Additionally, in a humanized tau mouse model, total loss of *Trem2* has been shown to worsen tau pathology [30]. The causes of these discrepancies are not well understood but may stem from differences in tau levels and isoforms expressed in various mouse models, as well as the timing of observations, such as early versus late stages of pathology. These inconsistencies also highlight a critical question: should therapeutic strategies aim to inhibit microglial activation or enhance it to effectively address tau pathology? In our study, although total *TREM2* mRNA levels increased approximately twofold - sufficient to drive robust microglial activation - the resulting impact on tau pathology and neurodegeneration in the PS19 background was only modestly beneficial. Therefore, our findings suggest that elevating TREM2 expression to activate microglia leads to mild improvements in tau pathology and neurodegeneration prevention.

AD is a complex chronic disorder involving multiple pathogenic pathways, including amyloid and tau proteinopathy, among others. Evaluating the therapeutic effects of targeting TREM2 in both amyloid and tau contexts is essential. TREM2 has been shown to play a key role in regulating microglial responses to Aβ deposition in many studies using amyloid mouse models [47–50]. Our previous work with TREM2-inducible mouse models in the 5xFAD background demonstrated that increasing TREM2-WT expression reduces amyloid deposition and neuritic dystrophy during the early stages of amyloid seeding [17]. However, a separate study using 5xFAD mice with AD-tau injections reported that chronic administration of an activating TREM2 antibody increased peri-plaque tau pathology and neuritic dystrophy, without altering Aβ plaque burden [27]. These findings raise important questions about whether elevating TREM2 expression or activating TREM2-mediated microglial functions would be beneficial in the context of both amyloid and tau pathologies, and what the optimal timing for such interventions might be. Further research is needed to clarify these issues.

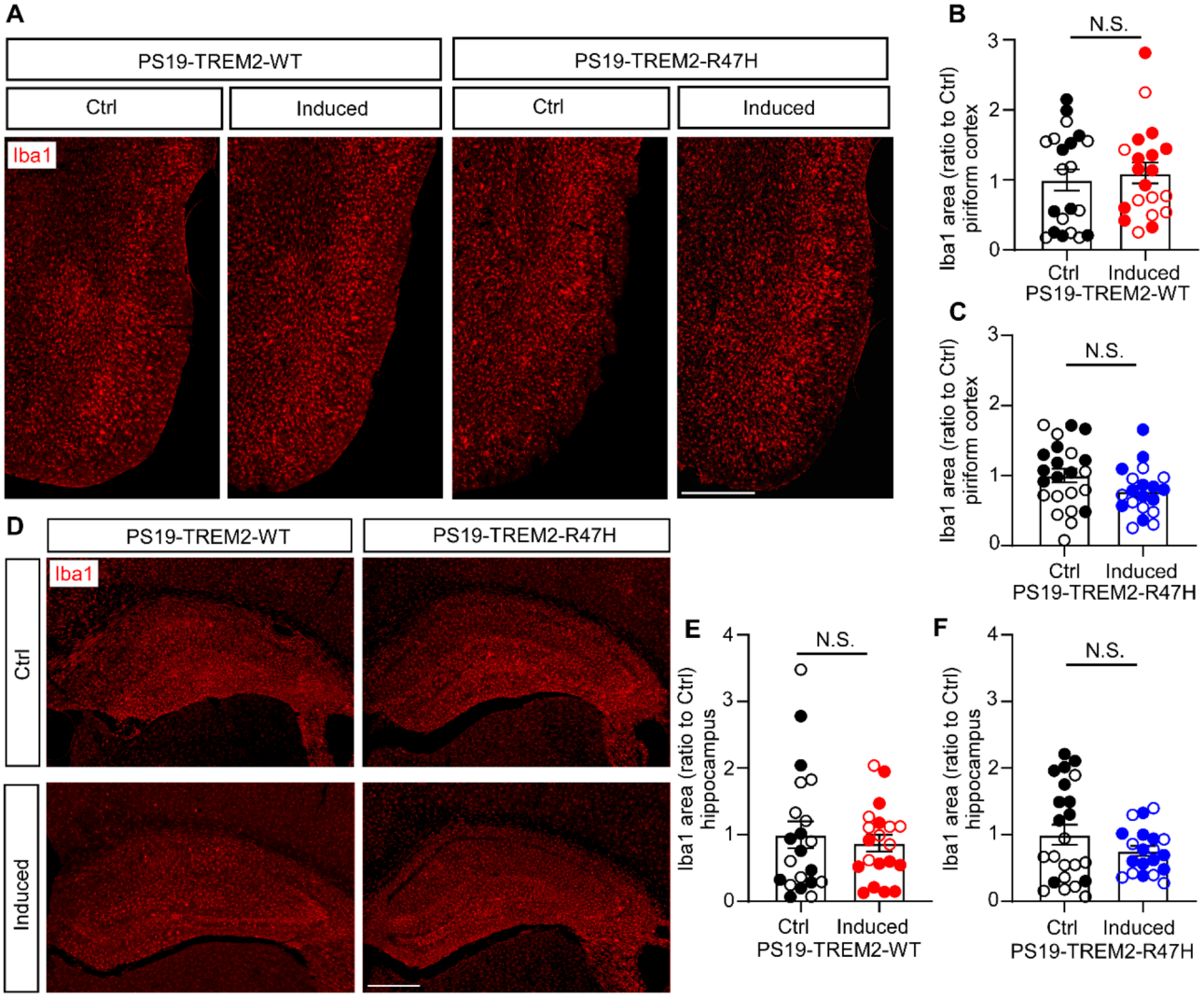

Fig. 4 TREM2 expression does not alter microglia density

(**A**-**C**) Representative images of piriform cortical region (**A**) and quantification (**B** and **C**) of microgliosis by immunofluorescence staining with Iba1 antibody. Scale bar, 500 µm. (**D**-**F**) Representative images of hippocampus (**D**) and quantification (**E** and **F**) of microgliosis by Iba1 immunofluorescence staining. Scale bar, 500 µm. Sample size: $n = 19–23$ mice/group, with mixed sexes. Each datapoint (circle) represents an individual animal, male and female mice are labeled as solid and open circles, respectively. Data are shown as mean ± SEM. Mann-Whitney tests were used for statistical analysis. *P* values < 0.05 were considered to be statistically significant. N.S., not significant.

ScRNA-seq studies have revealed that microglia are highly heterogeneous and identified a distinct DAM cluster in amyloid mouse models. These DAM cells were found to co-localize with Aβ plaques and are suggested to play a neuroprotective role by limiting amyloid deposition and reducing associated neurotoxicity. Studies have shown that deletion of *Trem2* leads to a depletion of the DAM phenotype in amyloid mouse models, indicating that TREM2 is a key regulator of DAM activation. Interestingly, DAM-like microglia have also been discovered and found to be enriched in PS19 tauopathy mice [51], however, whether TREM2 regulates DAM activation in tauopathy models remains unclear. Our scRNA-seq findings from PS19 mice confirmed that elevating TREM2-WT expression drives the activation of a DAM-like transcriptional signature, suggesting that TREM2-WT is capable of inducing a DAM-like phenotype in the context of tau pathology. Despite robust DAM activation, the effects on tau pathology and neurodegeneration in PS19 mice were relatively mild. This indicates that while TREM2-WT promotes microglial activation, its ability to mitigate tau-related pathology may be limited in a pure tauopathy model lacking amyloid deposition. This hypothesis is supported by a recent study showing that *Trem2* deletion exacerbates tau pathology only when amyloid pathology is present [52], suggesting that TREM2's protective effects may require co-existing amyloid pathology to fully manifest. Additionally, increasing

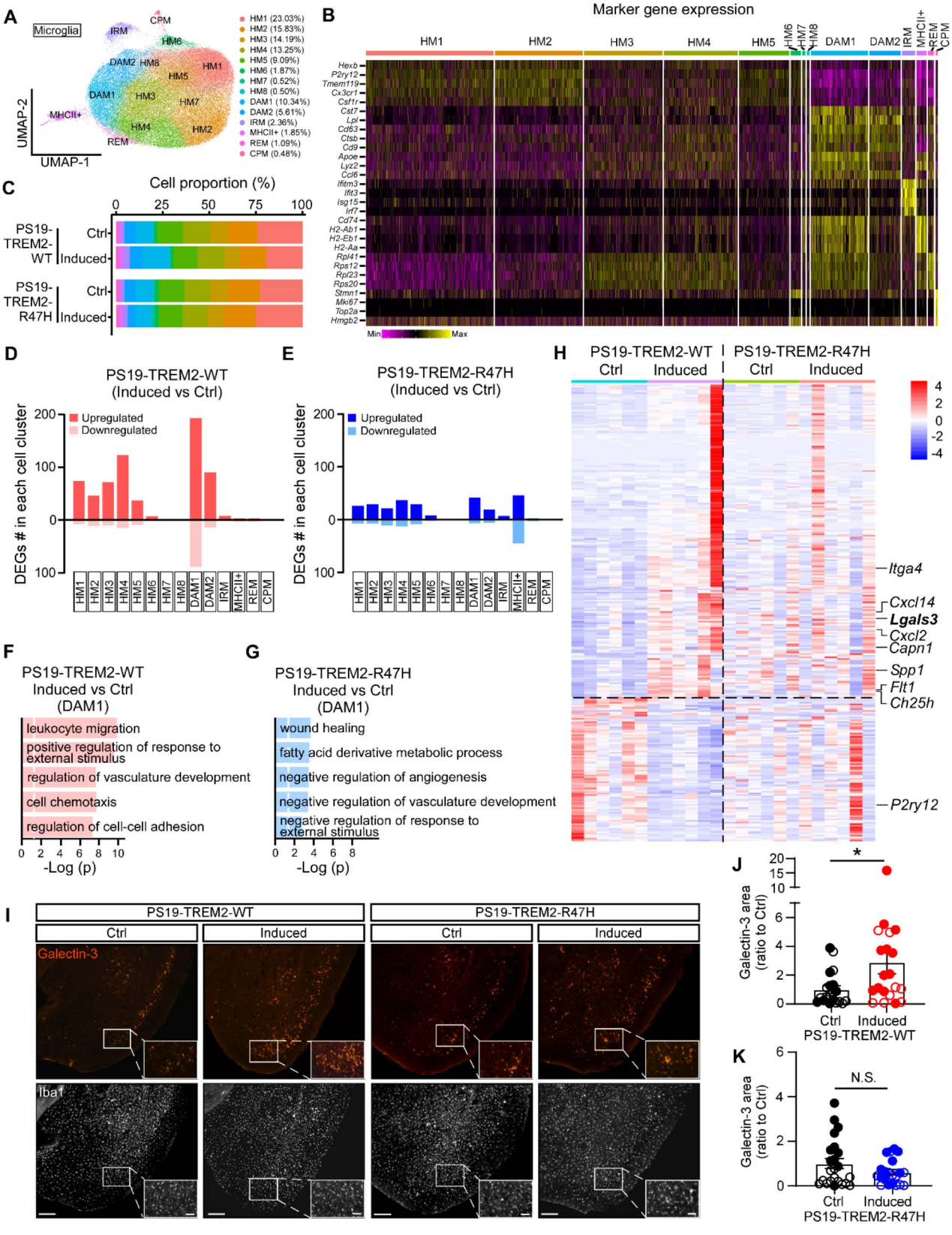

Fig. 5 (See legend on next page.)

(See figure on previous page.)

Fig. 5 Distinct microglial responses in PS19-TREM2-WT and PS19-TREM2-R47H mice by scRNA-seq
(**A**) UMAP plot showing 14 distinct microglial subclusters from PS19-TREM2-WT and PS19-TREM2-R47H mice. $n = 6$ mice per group (equal male and female). (**B**) Heatmap displaying the expression of key marker genes used to identify microglial subclusters, including homeostatic microglia (HM1-8), disease-associated microglia (DAM1 and DAM2), interferon response microglia (IRM), MHCII + microglia, ribosomal gene-enriched microglia (REM), and cycling/proliferating microglia (CPM). (**C**) Bar plots illustrating the proportions of microglial subclusters in each of the four groups. (**D** and **E**) Number of DEGs for all the microglia subclusters in the comparison between induced versus Ctrl groups of PS19-TREM2-WT (**D**) or and PS19-TREM2-R47H (**E**) mice. (**F** and **G**) Top five canonical pathways enriched by DEGs from DAM1 cluster in the comparison between induced versus Ctrl groups of PS19-TREM2-WT (**F**) or PS19-TREM2-R47H (**G**) mice. The threshold of significant *P* value is 0.05. (**H**) Heatmap showing the gene expression of combined DEGs in the DAM1 cluster from PS19-TREM2-WT and PS19-TREM2-R47H mice. (**I**) Representative images showing Galectin-3 and IBA1 staining in piriform cortical region. Scale bar is 200 µm and 50 µm for insert. (**J** and **K**) The Galectin-3 coverage areas were quantified and compared. $n = 19$–23 mice/group, each datapoint (circle) represents an individual animal, male and female mice are labeled as solid and open circles, respectively. Data are shown as mean ± SEM. Mann-Whitney tests with Bonferroni correction were used for statistical analysis. *P* value < 0.05 was considered to be statistically significant. *, $P < 0.05$; N.S., not significant.

evidence suggests that Aβ and tau do not act independently but rather interact through shared pathways [53–55], leading to a self-reinforcing cycle of neurotoxicity and neuronal damage, which is the key driver of microglial activation [56, 57]. Future studies should focus on evaluating TREM2's therapeutic potential in the context of Aβ, tau, and neuronal damage.

The TREM2-R47H variant significantly increases the risk of late-onset AD [4, 5]. Studies with amyloid mouse models have shown that TREM2-R47H leads to decreased TREM2 signaling, fewer plaque-associated microglia, reduced expression of TREM2-dependent activation markers [7, 58]. Interestingly, a study using bacterial artificial chromosome (BAC) transgenic mouse mice expressing human TREM2 in the PS19 background revealed that TREM2-R47H conferred a protective effect against tau pathology and neurodegeneration compared to the TREM2 common variant [25]. This protective effect probably attributed to reduced microglial activation, which limits microglia-driven neuroinflammation, synaptic loss and neuronal damage [25]. In our study, we similarly found that elevating TREM2-R47H expression failed to promote microglial activation, further supporting the notion that TREM2-R47H results in a partial loss of TREM2 function. However, unlike the BAC transgenic human TREM2 mice, we did not observe any effect of TREM2-R47H expression on tau pathology or neurodegeneration. This discrepancy may be due to differences in genetic backgrounds between the two models. Notably, while the BAC mice lack the endogenous murine *Trem2* gene [25], our animal model retains it, allowing mouse *Trem2* to remain functionally active. Another possibility is that although we overexpressed human TREM2-WT or TREM2-R47H in the mouse brain, the major TREM2 interactors, including DAP12, CD33, and APOE [16, 59–61], were all of murine origin. These proteins are key regulators of microglial activation, lipid metabolism, and immune signaling, and structural and functional differences between their human and mouse counterparts could impact TREM2 signaling efficiency [62–64], potentially dampening the effects of human TREM2-WT and TREM2-R47H in this study.

In summary, using our inducible mouse models, we demonstrate that elevating TREM2-WT levels activates strong microglial DAM signatures, but the impact on tau pathology and neurodegeneration is modest. Further studies are needed to investigate the effects of TREM2 in both amyloid and tau backgrounds to explore its full therapeutic potential for AD treatment.

Supplementary information

The online version contains supplementary material available at https://doi.org/10.1186/s12974-025-03420-8.

Supplementary Figure
Supplementary Figures 1–3
Supplementary Table 1
Supplementary Table 2
Supplementary Table 3
Supplementary Table 4

Acknowledgements
Not applicable.

Author contributions
K.C., F.L., G.B., and N.Z. developed the research concept and designed the experiments; K.C. and F.L. prepared the animals and tissues and performed the majority of experiments including immunofluorescence staining, Western blotting, and ELISA; Y. C. helped with animal breeding, genotyping, tamoxifen treatment and tissue collection; K.C., F.L. and Y.A.M. performed the single-cell isolation and library preparation; S.Z. and T.C.I. performed the statistical and bioinformatics analysis for scRNA-seq; Z.L., W.Q., A.D.M., Y.Z. and G.X. helped with sample preparation, immunofluorescence staining, image scanning and quantification; K.C. and N.Z. wrote the manuscript with critical inputs and edits by all the co-authors.

Funding
This work was supported by NIH grants R01AG66395, RF1AG056130, R01AG087165, and U19AG069701; a BrightFocus Foundation grant; and a grant from Cure Alzheimer's Fund (to N.Z.).

Data availability
Count matrices, raw sequencing data, and the metadata associated with each sample identifier are available in the National Center for Biotechnology Information Gene Expression Omnibus under accession number GSE285713.

Declarations

Ethics approval and consent to participate
All animal procedures were approved by the Mayo Clinic Institutional Animal Care and Use Committee (IACUC) and in compliance with the National Institutes of Health (NIH) Guidelines for the Care and Use of Laboratory Animals.

Consent for publication
All the authors approved the final version for publication.

Competing interests
G.B. serves as a consultant for SciNeuro Pharmaceuticals and Kisbee Therapeutics. Y.A.M. is a current employee of SciNeuro Pharmaceuticals.

Received: 8 January 2025 / Accepted: 17 March 2025
Published online: 23 March 2025

References

1. Wilson DM 3rd, Cookson MR, Van Den Bosch L, Zetterberg H, Holtzman DM, Dewachter I. Hallmarks of neurodegenerative diseases. Cell. 2023;186:693–714.
2. Thal DR, von Arnim C, Griffin WS, Yamaguchi H, Mrak RE, Attems J, Upadhaya AR. Pathology of clinical and preclinical Alzheimer's disease. Eur Arch Psychiatry Clin Neurosci. 2013;263(2):S137–145.
3. Itagaki S, McGeer PL, Akiyama H, Zhu S, Selkoe D. Relationship of microglia and astrocytes to amyloid deposits of Alzheimer disease. J Neuroimmunol. 1989;24:173–82.
4. Guerreiro R, Wojtas A, Bras J, Carrasquillo M, Rogaeva E, Majounie E, Cruchaga C, Sassi C, Kauwe JS, Younkin S, et al. TREM2 variants in Alzheimer's disease. N Engl J Med. 2013;368:117–27.
5. Jonsson T, Stefansson H, Steinberg S, Jonsdottir I, Jonsson PV, Snaedal J, Bjornsson S, Huttenlocher J, Levey AI, Lah JJ, et al. Variant of TREM2 associated with the risk of Alzheimer's disease. N Engl J Med. 2013;368:107–16.
6. Ulrich JD, Ulland TK, Colonna M, Holtzman DM. Elucidating the Role of TREM2 in Alzheimer's Disease. Neuron. 2017;94:237–48.
7. Wang Y, Cella M, Mallinson K, Ulrich JD, Young KL, Robinette ML, Gilfillan S, Krishnan GM, Sudhakar S, Zinselmeyer BH, et al. TREM2 lipid sensing sustains the microglial response in an Alzheimer's disease model. Cell. 2015;160:1061–71.
8. Song W, Hooli B, Mullin K, Jin SC, Cella M, Ulland TK, Wang Y, Tanzi RE, Colonna M. Alzheimer's disease-associated TREM2 variants exhibit either decreased or increased ligand-dependent activation. Alzheimers Dement. 2017;13:381–7.
9. Zhao Y, Wu X, Li X, Jiang LL, Gui X, Liu Y, Sun Y, Zhu B, Pina-Crespo JC, Zhang M, et al. TREM2 Is a Receptor for beta-Amyloid that Mediates Microglial Function. Neuron. 2018;97:1023–e10311027.
10. Zhong L, Wang Z, Wang D, Wang Z, Martens YA, Wu L, Xu Y, Wang K, Li J, Huang R, et al. Amyloid-beta modulates microglial responses by binding to the triggering receptor expressed on myeloid cells 2 (TREM2). Mol Neurodegener. 2018;13:15.
11. Xing J, Titus AR, Humphrey MB. The TREM2-DAP12 signaling pathway in Nasu-Hakola disease: a molecular genetics perspective. Res Rep Biochem. 2015;5:89–100.
12. Ulland TK, Song WM, Huang SC, Ulrich JD, Sergushichev A, Beatty WL, Loboda AA, Zhou Y, Cairns NJ, Kambal A, et al. TREM2 maintains microglial metabolic fitness in Alzheimer's disease. Cell. 2017;170:649–e663613.
13. Konishi H, Kiyama H. Microglial TREM2/DAP12 Signaling: a double-edged sword in neural diseases. Front Cell Neurosci. 2018;12:206.
14. Pimenova AA, Marcora E, Goate AM. A Tale of Two Genes: Microglial Apoe and Trem2. Immunity. 2017;47:398–400.
15. Keren-Shaul H, Spinrad A, Weiner A, Matcovitch-Natan O, Dvir-Szternfeld R, Ulland TK, David E, Baruch K, Lara-Astaiso D, Toth B, et al. A unique microglia type associated with restricting development of Alzheimer's disease. Cell. 2017;169:1276–e12901217.
16. Krasemann S, Madore C, Cialic R, Baufeld C, Calcagno N, El Fatimy R, Beckers L, O'Loughlin E, Xu Y, Fanek Z, et al. The TREM2-APOE pathway drives the transcriptional phenotype of dysfunctional microglia in neurodegenerative diseases. Immunity. 2017;47:566–e581569.
17. Zhao N, Qiao W, Li F, Ren Y, Zheng J, Martens YA, Wang X, Li L, Liu CC, Chen K et al. Elevating microglia TREM2 reduces amyloid seeding and suppresses disease-associated microglia. J Exp Med. 2022;219.
18. Deczkowska A, Weiner A, Amit I. The Physiology, Pathology, and Potential Therapeutic Applications of the TREM2 Signaling Pathway. Cell. 2020;181:1207–17.
19. Lee CYD, Daggett A, Gu X, Jiang LL, Langfelder P, Li X, Wang N, Zhao Y, Park CS, Cooper Y, et al. Elevated TREM2 Gene Dosage Reprograms Microglia Responsivity and Ameliorates Pathological Phenotypes in Alzheimer's Disease Models. Neuron. 2018;97:1032–e10481035.
20. Wang S, Mustafa M, Yuede CM, Salazar SV, Kong P, Long H, Ward M, Siddiqui O, Paul R, Gilfillan S et al. Anti-human TREM2 induces microglia proliferation and reduces pathology in an Alzheimer's disease model. J Exp Med. 2020;217.
21. Schlepckow K, Monroe KM, Kleinberger G, Cantuti-Castelvetri L, Parhizkar S, Xia D, Willem M, Werner G, Pettkus N, Brunner B, et al. Enhancing protective microglial activities with a dual function TREM2 antibody to the stalk region. EMBO Mol Med. 2020;12:e11227.
22. Zhao P, Xu Y, Jiang L, Fan X, Li L, Li X, Arase H, Zhao Y, Cao W, Zheng H, et al. A tetravalent TREM2 agonistic antibody reduced amyloid pathology in a mouse model of Alzheimer's disease. Sci Transl Med. 2022;14:eabq0095.
23. Zhao N, Bu G. A TREM2 antibody energizes microglia. Nat Neurosci. 2023;26:366–8.
24. van Lengerich B, Zhan L, Xia D, Chan D, Joy D, Park JI, Tatarakis D, Calvert M, Hummel S, Lianoglou S, et al. A TREM2-activating antibody with a blood-brain barrier transport vehicle enhances microglial metabolism in Alzheimer's disease models. Nat Neurosci. 2023;26:416–29.
25. Gratuze M, Leyns CE, Sauerbeck AD, St-Pierre MK, Xiong M, Kim N, Serrano JR, Tremblay ME, Kummer TT, Colonna M, et al. Impact of TREM2R47H variant on tau pathology-induced gliosis and neurodegeneration. J Clin Invest. 2020;130:4954–68.
26. Leyns CEG, Ulrich JD, Finn MB, Stewart FR, Koscal LJ, Remolina Serrano J, Robinson GO, Anderson E, Colonna M, Holtzman DM. TREM2 deficiency attenuates neuroinflammation and protects against neurodegeneration in a mouse model of tauopathy. Proc Natl Acad Sci U S A. 2017;114:11524–9.
27. Jain N, Lewis CA, Ulrich JD, Holtzman DM. Chronic TREM2 activation exacerbates Abeta-associated tau seeding and spreading. J Exp Med. 2023;220.
28. Zhu B, Liu Y, Hwang S, Archuleta K, Huang H, Campos A, Murad R, Pina-Crespo J, Xu H, Huang TY. Trem2 deletion enhances tau dispersion and pathology through microglia exosomes. Mol Neurodegener. 2022;17:58.
29. Lee SH, Meilandt WJ, Xie L, Gandham VD, Ngu H, Barck KH, Rezzonico MG, Imperio J, Lalehzadeh G, Huntley MA, et al. Trem2 restrains the enhancement of tau accumulation and neurodegeneration by beta-amyloid pathology. Neuron. 2021;109:1283–e13011286.
30. Bemiller SM, McCray TJ, Allan K, Formica SV, Xu G, Wilson G, Kokiko-Cochran ON, Crish SD, Lasagna-Reeves CA, Ransohoff RM, et al. TREM2 deficiency exacerbates tau pathology through dysregulated kinase signaling in a mouse model of tauopathy. Mol Neurodegener. 2017;12:74.
31. Sayed FA, Telpoukhovskaia M, Kodama L, Li Y, Zhou Y, Le D, Hauduc A, Ludwig C, Gao F, Clelland C, et al. Differential effects of partial and complete loss of TREM2 on microglial injury response and tauopathy. Proc Natl Acad Sci U S A. 2018;115:10172–7.
32. Parkhurst CN, Yang G, Ninan I, Savas JN, Yates JR 3rd, Lafaille JJ, Hempstead BL, Littman DR, Gan WB. Microglia promote learning-dependent synapse formation through brain-derived neurotrophic factor. Cell. 2013;155:1596–609.
33. Liu CC, Yamazaki Y, Heckman MG, Martens YA, Jia L, Yamazaki A, Diehl NN, Zhao J, Zhao N, DeTure M, et al. Tau and apolipoprotein E modulate cerebrovascular tight junction integrity independent of cerebral amyloid angiopathy in Alzheimer's disease. Alzheimers Dement. 2020;16:1372–83.
34. Jicha GA, Bowser R, Kazam IG, Davies P. Alz-50 and MC-1, a new monoclonal antibody raised to paired helical filaments, recognize conformational epitopes on recombinant tau. J Neurosci Res. 1997;48:128–32.
35. Sala Frigerio C, Wolfs L, Fattorelli N, Thrupp N, Voytyuk I, Schmidt I, Mancuso R, Chen WT, Woodbury ME, Srivastava G, et al. The Major Risk Factors for Alzheimer's Disease: Age, Sex, and Genes Modulate the Microglia Response to Aβ Plaques. Cell Rep. 2019;27:1293–e13061296.
36. Xu S, Hu E, Cai Y, Xie Z, Luo X, Zhan L, Tang W, Wang Q, Liu B, Wang R, et al. Using clusterProfiler to characterize multiomics data. Nat Protoc. 2024;19:3292–320.
37. Wu T, Hu E, Xu S, Chen M, Guo P, Dai Z, Feng T, Zhou L, Tang W, Zhan L, et al. clusterProfiler 4.0: A universal enrichment tool for interpreting omics data. Innov (Camb). 2021;2:100141.

38. Holmes BB, Furman JL, Mahan TE, Yamasaki TR, Mirbaha H, Eades WC, Belaygorod L, Cairns NJ, Holtzman DM, Diamond MI. Proteopathic tau seeding predicts tauopathy in vivo. Proc Natl Acad Sci U S A. 2014;111:E4376–4385.
39. Yoshiyama Y, Higuchi M, Zhang B, Huang SM, Iwata N, Saido TC, Maeda J, Suhara T, Trojanowski JQ, Lee VM. Synapse loss and microglial activation precede tangles in a P301S tauopathy mouse model. Neuron. 2007;53:337–51.
40. Faust TE, Feinberg PA, O'Connor C, Kawaguchi R, Chan A, Strasburger H, Frosch M, Boyle MA, Masuda T, Amann L, et al. A comparative analysis of microglial inducible Cre lines. Cell Rep. 2023;42:113031.
41. Shi Y, Yamada K, Liddelow SA, Smith ST, Zhao L, Luo W, Tsai RM, Spina S, Grinberg LT, Rojas JC, et al. ApoE4 markedly exacerbates tau-mediated neurodegeneration in a mouse model of tauopathy. Nature. 2017;549:523–7.
42. Sala Frigerio C, Wolfs L, Fattorelli N, Thrupp N, Voytyuk I, Schmidt I, Mancuso R, Chen WT, Woodbury ME, Srivastava G, et al. The Major Risk Factors for Alzheimer's Disease: Age, Sex, and Genes Modulate the Microglia Response to Abeta Plaques. Cell Rep. 2019;27:1293–e13061296.
43. Ellwanger DC, Wang S, Brioschi S, Shao Z, Green L, Case R, Yoo D, Weishuhn D, Rathanaswami P, Bradley J et al. Prior activation state shapes the microglia response to antihuman TREM2 in a mouse model of Alzheimer's disease. Proc Natl Acad Sci USA. 2021;118.
44. Pichet Binette A, Franzmeier N, Spotorno N, Ewers M, Brendel M, Biel D, Alzheimer's Disease Neuroimaging I, Strandberg O, Janelidze S, Palmqvist S, et al. Amyloid-associated increases in soluble tau relate to tau aggregation rates and cognitive decline in early Alzheimer's disease. Nat Commun. 2022;13:6635.
45. Jiang T, Tan L, Zhu X-C, Zhou J-S, Cao L, Tan M-S, Wang H-F, Chen Q, Zhang Y-D, Yu J-T. Silencing of TREM2 exacerbates tau pathology, neurodegenerative changes, and spatial learning deficits in P301S tau transgenic mice. Neurobiol Aging. 2015;36:3176–86.
46. Jiang T, Zhang YD, Gao Q, Ou Z, Gong PY, Shi JQ, Wu L, Zhou JS. TREM2 Ameliorates Neuronal Tau Pathology Through Suppression of Microglial Inflammatory Response. Inflammation. 2018;41:811–23.
47. Jay TR, Hirsch AM, Broihier ML, Miller CM, Neilson LE, Ransohoff RM, Lamb BT, Landreth GE. Disease Progression-Dependent Effects of TREM2 Deficiency in a Mouse Model of Alzheimer's Disease. J Neurosci. 2017;37:637–47.
48. Jay TR, Miller CM, Cheng PJ, Graham LC, Bemiller S, Broihier ML, Xu G, Margevicius D, Karlo JC, Sousa GL, et al. TREM2 deficiency eliminates TREM2 + inflammatory macrophages and ameliorates pathology in Alzheimer's disease mouse models. J Exp Med. 2015;212:287–95.
49. Parhizkar S, Arzberger T, Brendel M, Kleinberger G, Deussing M, Focke C, Nuscher B, Xiong M, Ghasemigharagoz A, Katzmarski N, et al. Loss of TREM2 function increases amyloid seeding but reduces plaque-associated ApoE. Nat Neurosci. 2019;22:191–204.
50. Wang Y, Ulland TK, Ulrich JD, Song W, Tzaferis JA, Hole JT, Yuan P, Mahan TE, Shi Y, Gilfillan S, et al. TREM2-mediated early microglial response limits diffusion and toxicity of amyloid plaques. J Exp Med. 2016;213:667–75.
51. Shi Y, Andhey PS, Ising C, Wang K, Snipes LL, Boyer K, Lawson S, Yamada K, Qin W, Manis M, et al. Overexpressing low-density lipoprotein receptor reduces tau-associated neurodegeneration in relation to apoE-linked mechanisms. Neuron. 2021;109:2413–e24262417.
52. Lee SH, Meilandt WJ, Xie L, Gandham VD, Ngu H, Barck KH, Rezzonico MG, Imperio J, Lalehzadeh G, Huntley MA, et al. Trem2 restrains the enhancement of tau accumulation and neurodegeneration by β-amyloid pathology. Neuron. 2021;109:1283–e13011286.
53. Busche MA, Hyman BT. Synergy between amyloid-β and tau in Alzheimer's disease. Nat Neurosci. 2020;23:1183–93.
54. Small SA, Duff K. Linking Abeta and tau in late-onset Alzheimer's disease: a dual pathway hypothesis. Neuron. 2008;60:534–42.
55. Zheng WH, Bastianetto S, Mennicken F, Ma W, Kar S. Amyloid beta peptide induces tau phosphorylation and loss of cholinergic neurons in rat primary septal cultures. Neuroscience. 2002;115:201–11.
56. Dolan MJ, Therrien M, Jereb S, Kamath T, Gazestani V, Atkeson T, Marsh SE, Goeva A, Lojek NM, Murphy S, et al. Exposure of iPSC-derived human microglia to brain substrates enables the generation and manipulation of diverse transcriptional states in vitro. Nat Immunol. 2023;24:1382–90.
57. Zia S, Hammond BP, Zirngibl M, Sizov A, Baaklini CS, Panda SP, Ho MFS, Lee KV, Mainali A, Burr MK, et al. Single-cell microglial transcriptomics during demyelination defines a microglial state required for lytic carcass clearance. Mol Neurodegener. 2022;17:82.
58. Song WM, Joshita S, Zhou Y, Ulland TK, Gilfillan S, Colonna M. Humanized TREM2 mice reveal microglia-intrinsic and -extrinsic effects of R47H polymorphism. J Exp Med. 2018;215:745–60.
59. Yuan P, Condello C, Keene CD, Wang Y, Bird TD, Paul SM, Luo W, Colonna M, Baddeley D, Grutzendler J. TREM2 Haplodeficiency in Mice and Humans Impairs the Microglia Barrier Function Leading to Decreased Amyloid Compaction and Severe Axonal Dystrophy. Neuron. 2016;90:724–39.
60. Colonna M. The biology of TREM receptors. Nat Rev Immunol. 2023;23:580–94.
61. Griciuc A, Patel S, Federico AN, Choi SH, Innes BJ, Oram MK, Cereghetti G, McGinty D, Anselmo A, Sadreyev RI, et al. TREM2 Acts Downstream of CD33 in Modulating Microglial Pathology in Alzheimer's Disease. Neuron. 2019;103:820–e835827.
62. Maloney B, Ge YW, Alley GM, Lahiri DK. Important differences between human and mouse APOE gene promoters: limitation of mouse APOE model in studying Alzheimer's disease. J Neurochem. 2007;103:1237–57.
63. Tchilian EZ, Beverley PC, Young BD, Watt SM. Molecular cloning of two isoforms of the murine homolog of the myeloid CD33 antigen. Blood. 1994;83:3188–98.
64. Brinkman-Van der Linden EC, Angata T, Reynolds SA, Powell LD, Hedrick SM, Varki A. CD33/Siglec-3 binding specificity, expression pattern, and consequences of gene deletion in mice. Mol Cell Biol. 2003;23:4199–206.

Publisher's note